2024 IEEE/RSJ International Conference on Intelligent Robots and Systems (IROS)
October 14-18, 2024. Abu Dhabi, UAE

The Control Strategy for Vehicle Transfer Robots in RO/RO Terminal Environments

Zhi Liu, Yongkang Xu, Lin Zhang, Shoukun Wang and Junzheng Wang

***Abstract*— In the labor-intensive Roll-On/Roll-Off (RO/RO) terminal environment, research on vehicle transport robots with mobility, stability, and reliability is receiving increasing attention. This paper presents a novel control framework for a Straddle-Type Dual-Body vehicle transfer robot. Initially, fine segmentation and processing of point clouds from different areas of the robot are performed, switching perception strategies for different areas based on event triggers. For target pose estimation, a traversal-based point cloud matrix fitting algorithm is designed. Additionally, for loading and unloading operations, a docking controller based on real-time target detection is developed to ensure minimal lateral and angular errors during target docking. Finally, the proposed control framework is validated through operations of the vehicle transfer robot in outdoor RO/RO terminal yards. Experimental results indicate that the average docking error remains within $3cm$, with a 6.5% reduction in docking time under the same conditions. The docking precision and stability performance of the vehicle transfer robot surpass traditional methods, demonstrating satisfactory performance.**

I. INTRODUCTION

As a pivotal transit hub for both maritime and land-based logistics, ports handle 85% of global logistics tasks. Automobile transfer operations at Roll-On/Roll-Off (RO/RO) terminals are crucial to port logistics[1]. In RO/RO terminals' challenging environments, human drivers face issues like low efficiency, high costs, safety hazards, and environmental pressures[2]. Thus, developing robots for vehicle transfer operations at RO/RO terminals holds great potential.

In the industrial transportation sector, various types of handling robots play a significant role and are widely utilized[3]. For instance, indoor-operating forklift robots were introduced for pallet handling tasks in [4]. Additionally, [5] presents an automated manufacturing system tailored for flexible workshops, enabling material transfer operations within the workshop. Moreover, [6] details the development of a decentralized and efficient cooperation system to guide indoor handling robots.

In response to the growing demand for commercial vehicle transportation, robots must meet higher safety and precision standards. These robots include underbody carriers, transverse forklifts, and longitudinal loaders. [7] describes an underbody carrier robot for indoor flat environments, but it lacks vehicle recognition capability. [8] presents a longitudinal loading robot using Lyapunov-based control for navigating narrow lanes. [9] developed a transverse forklift robot for commercial vehicle transfers. Path planning for transverse forklift robots was studied in [10], while [11] investigates multi-vehicle coordination for underbody carrier robots.

This study focuses on investigating a Straddle-Type Dual-Body robot designed for vehicle transport in unstructured environments at RO/RO terminals. This robot offers several advantages, including low environmental requirements, high parking density, rapid travel speed, and minimal parking lot modifications. The primary focus of the control strategy research lies in detecting target vehicle poses and controlling robot-to-vehicle docking.

Pose estimation algorithms for handling robots use various types of information, including visual, radar[12], depth, and pressure data. For instance, [13] proposed a convolutional deep network algorithm based on radar information for maritime mobile robot docking. In [14], visual recognition combined with depth information from point clouds was used for automatic positioning of vehicle components in painting robots. [15] introduced a robot grasping system using multi-view depth images for visual target pose acquisition. Additionally, [16] investigated a convolutional neural network algorithm using binocular images for fruit detection and pose estimation. [17] proposed a method using touch for pose estimation, while [9] introduced a system based on a pressure sensor array, though it had limited accuracy for vehicle pose estimation.

Several strategies for robot docking control focus on error correction and path-planning[18]. For instance, [19] used laser scanning data to detect angle and distance deviations, designing control laws for error correction. Similarly, [20] employed visual recognition to identify pallets and tracked their pose to facilitate docking. [21] used a fifth-order polynomial to generate forklift trajectories for precise pallet positioning. [22] utilized continuous curvature turning to create high-quality paths for accurate docking. Lastly, [23] generated continuous curvature paths for docking maneuvers, followed by path tracking control to adhere to predefined routes.

This article presents a novel control framework for a Straddle-Type Dual-Body vehicle transfer robot, designed for efficient goods handling and vehicle transfer operations. The main contributions are:

1) A control framework is developed for a Straddle-type Dual-body vehicle transport robot, which includes a range detection strategy switching algorithm based on event triggering, a target attitude observer based on

This work is supported by the Fundamental Research Funds for the Central Universities under Grant 2024CX06030. (Corresponding author: Shoukun Wang)

All authors are with School of Automation,Beijing institute of technology, 100081, Beijing, China. (3220220790@bit.edu.cn)

LIDAR, and a docking controller based on real-time detection, for challenging transportation operations in unstructured environments.

2) Extensive experimentation validates the effectiveness and engineering applicability of our developed control framework for the straddle-type vehicle transport robot, particularly in navigating unstructured terrains within RO/RO terminals.

The structure of the remaining sections is as follows: Section II provides an overview of the vehicle transfer robot system and its kinematic model. Section III introduces the control strategy. In Section IV, we demonstrate the method's effectiveness through three field tests. Finally, Section V summarizes the study's contributions.

II. Robot System

In non-structured environments like RO/RO terminals, the Straddle-Type Dual-Body robot offers flexible movement and minimal environmental constraints. With four clamping mechanisms inside the cavities, the robot efficiently and stably executes vehicle transfers. This paper introduces the development of this robot, shown in Fig. 1. It can swiftly traverse uneven surfaces with loaded vehicles and maneuver flexibly in congested yards.

The straddle-type dual-body vehicle transport robot comprises a chassis, perception system, four-wheel independent drive steering system, clamping mechanism, and power system. The perception system includes multi-line LIDARs around the robot and four single-line LIDARs on the clamping mechanism. The clamping mechanism grips the target vehicle's tires during loading and unloading. The four-wheel drive system enables steering, self-rotation, and lateral movement. The power system provides energy, while the communication network includes CAN bus, RS232, and a 5G module.

III. Robot Control Strategy

A. Robot kinematic model

The system structure and kinematic model of the vehicle transport robot were analyzed previously. This section discusses the control strategy, including four parts: Event-Triggered Range Detection Strategy Switch Algorithm (ETRDSSA), Target Vehicle Pose Estimation Algorithm (TVPEA), and Real-Time Target Measurement Docking Controller (RTTMDC), as shown in Fig. 2.

Fig. 1: The structure of the vehicle transfer robot system

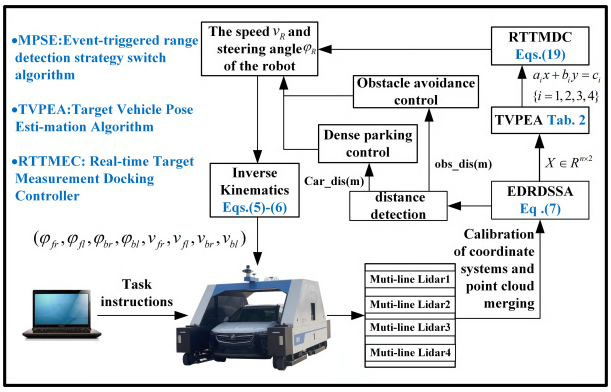

Fig. 2: Vehicle Transfer Robot Control Diagram

B. Event-triggered range detection strategy switch algorithm

The robot's environmental detection aims at target identification and obstacle recognition. ETRDSSA addresses two key challenges: First, LiDAR struggles to distinguish between target vehicles and obstacles compared to visual data. Second, effective obstacle avoidance requires considering the robot's motion mode, task type, and current stage.

ETRDSSA divides the robot's omnidirectional perception area into various ranges: front and rear central, edge, and corner areas; left and right side areas; and internal front and rear areas, as shown in Fig. 3. An event-triggered mechanism then applies different control strategies based on the vehicle's state, including target detection, obstacle detection, and ignoring. This mechanism facilitates strategy changes under specific conditions:

$$x \in \Psi = \{x \in states \mid t = T_i, d = D_j, p = P_t\}, \quad (1)$$

where Psi represents different control strategies for various detection regions, T_i denotes task types (pick-up, drop-off, movement), D_j signifies motion directions (rotation, four-wheel straight, lateral movement), and P_t indicates robot stages (navigation, pick-up, drop-off). The trigger conditions are as follows: during navigation, the robot focuses on obstacle detection based on its motion direction; during pick-up, it detects targets and controls obstacles in the front region; and during drop-off, it performs target detection and obstacle control in the front region.

C. Target Vehicle Pose Estimation Algorithm

When using multi-line lidar for long-distance detection, vehicle transport robots can only detect the target vehicle's outline facing the lidar. TVPEA uses a search-based approach to approximate the best-fit rectangle, estimating the vehicle's relative pose, as shown in TABLE 1.

TVPEA is a traversal-based matrix fitting method that estimates the pose of vehicles using range data points X,

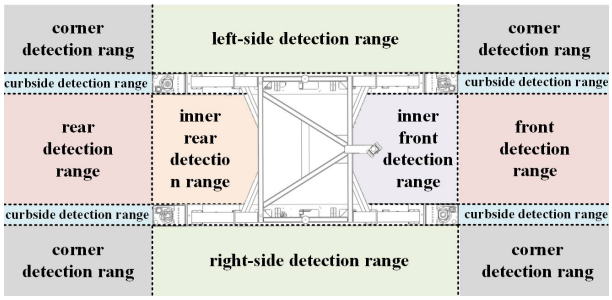

Fig. 3: Point Cloud Refinement Segmentation and Processing

TABLE I: Main technical indicators of the vehicle transport robot

Algorithm Traversal-Based Matrix Fitting Target Pose Estimation Algorithm

Input: range data points $X \in R^{n\times 2}$
Output: rectangle edges $\{a_i x + b_i y = c_i \mid i = 1, 2, 3, 4\}$
$Q \longleftarrow \phi$
for $\theta = 0$ to $\pi/2 - \delta$ step δ do
$\hat{e}_1 \leftarrow (cos\theta, sin\theta)$
$\hat{e}_2 \leftarrow (-sin\theta, cos\theta)$
$C_1 \leftarrow X \cdot \hat{e}_1^T$
$C_2 \leftarrow X \cdot \hat{e}_2^T$
$c_1^{max} \leftarrow max\{C_1\}$, $c_1^{min} \leftarrow min\{C_1\}$
$c_2^{max} \leftarrow max\{C_2\}$, $c_2^{min} \leftarrow min\{C_2\}$
$a \leftarrow -(c_1^{max} - c_1^{min}) \cdot (c_2^{max} - c_2^{min})$
insert a into Q with key (θ)
end for
select key (θ^*) from Q with maximum value
$C_1^* \leftarrow X \cdot (cos\theta^*, sin\theta^*)^T$, $C_2^* \leftarrow X \cdot (-sin\theta^*, cos\theta^*)^T$
$a_1 \leftarrow cos\theta^*$, $b_1 \leftarrow sin\theta^*$, $c_1 \leftarrow min\{C_1^*\}$
$a_2 \leftarrow -sin\theta^*$, $b_2 \leftarrow cos\theta^*$, $c_2 \leftarrow min\{C_2^*\}$
$a_3 \leftarrow cos\theta^*$, $b_3 \leftarrow sin\theta^*$, $c_3 \leftarrow max\{C_1^*\}$
$a_4 \leftarrow -sin\theta^*$, $b_4 \leftarrow cos\theta^*$, $c_4 \leftarrow max\{C_2^*\}$

where $X \in \mathbb{R}^{n\times 2}$ represents the point cloud data in the laser coordinate system. The algorithm projects X onto various angles, calculating maximum and minimum values, and an evaluation criterion a, to determine the vehicle's position and orientation on the plane. The criterion a is computed using the maximum c_1^{max} and minimum c_1^{min} values along one projection direction, and the maximum c_2^{max} and minimum c_2^{min} values along the perpendicular direction. The difference $(c_1^{max}-c_1^{min})\cdot(c_2^{max}-c_2^{min})$ provides the evaluation criterion a, reflecting the shape and compactness of the vehicle's outline at angle θ. The algorithm then selects the angle θ^* with the maximum criterion and computes the four boundary points of the vehicle. This method accurately estimates the vehicle's pose using partial outline information, especially useful for long-distance detection.

D. Real-time Target Measurement Docking Controller

After obtaining the target pose in real time, the RTTMEC controller can generate the overall velocity and steering angle of the vehicle transport robot, enabling it to complete tasks such as picking up and dropping off vehicles.

The ideal robot is constructed, and discussions revolve around its motion planning. Upon acquiring the target pose, achieving a path with zero angular and lateral deviations is termed the safe path. Controlling the ideal robot to move along this safe path, the ultimate goal is to accomplish docking. The initial position of the ideal robot $(x_{ir,0}, y_{ir,0})$ is set on the safe path at the point closest to the robot. The motion trajectory of the ideal robot is as follows:

$$\begin{bmatrix} x_{ir} \\ y_{ir} \end{bmatrix} = \begin{bmatrix} x_{ir,0} \\ y_{ir,0} \end{bmatrix} + \begin{bmatrix} v_{ir} t sin\theta_T \\ v_{ir} t cos\theta_T \end{bmatrix} \tag{2}$$

where (x_{ir}, y_{ir}) is the position of the ideal robot, t is time, v_{ir} is the velocity of the ideal robot, and θ_T is the heading angle of the target vehicle.

The pose information of the robot can be obtained through GPS sensors, and the pose of the ideal robot in the robot coordinate system can be acquired.

$$\begin{aligned} \begin{bmatrix} {}^R x_{ir} \\ {}^R y_{ir} \end{bmatrix} &= \begin{bmatrix} \cos\theta_R & \sin\theta_R \\ -\sin\theta_R & \cos\theta_R \end{bmatrix} \begin{bmatrix} x_{ir} - x_R \\ y_{ir} - y_R \end{bmatrix}, \\ {}^R\theta_{ir} &= \theta_R - \theta_{ir}, \end{aligned} \tag{3}$$

where $({}^R x_{ir}, {}^R y_{ir})$ is the relative position of the ideal robot in the robot's coordinate system, (x_R, y_R, θ_R) is the robot's pose, and θ_{ir} is the ideal robot's heading angle.

After incorporating the relative pose of the target in the robot's coordinate system obtained by TVPEA into Equation 2, we can obtain:

$$\begin{bmatrix} {}^R x_{ir} \\ {}^R y_{ir} \end{bmatrix} = \begin{bmatrix} {}^R x_T \\ {}^R y_T \end{bmatrix} + \begin{bmatrix} \cos\theta_R & \sin\theta_R \\ \sin\theta_R & \cos\theta_R \end{bmatrix} \begin{bmatrix} x_T & x_{ir} \\ y_T & y_{ir} \end{bmatrix}. \tag{4}$$

where $({}^R x_T, {}^R y_T)$ is the relative position of the target in the robot's coordinate system and (x_T, y_T) is the position of the target.

Afterward, taking the derivative, we obtain:

$$\begin{aligned} {}^R\dot{x}_{ir} &= v_R \sin\varphi_R {}^R y_{ir}/r_R + v_{ir}\cos{}^R\theta_{ir} - v_R\cos\varphi_R, \\ {}^R\dot{y}_{ir} &= -v_R \sin\varphi_R {}^R x_{ir}/r_R - v_{ir}\sin{}^R\theta_{ir}, \\ {}^R\dot{\theta}_{ir} &= v_R \sin\varphi_R/r_R. \end{aligned} \tag{5}$$

where, ${}^R\theta_{ir}$ represents the actual values of the heading angle of the ideal robot in the robot coordinate system.

Due to the occasional relationship between v_R and φ_R, a new set of variables u_1 and u_2 is established. They are introduced into Eq. 5 as follows:

$$\begin{aligned} {}^R\dot{x}_{ir} &= u_1 {}^R y_{ir}/r_R + v_{ir}\cos{}^R\theta_{ir} - u_2, \\ {}^R\dot{y}_{ir} &= -u_1 {}^R x_{ir}/r_R - v_{ir}\sin{}^R\theta_{ir}, \\ {}^R\dot{\theta}_{ir} &= u_1/r_R. \end{aligned} \tag{6}$$

where $u_1 = v_R \sin\varphi_R$, $u_2 = v_R\cos\varphi_R$.

The difference between the actual heading angle of the ideal robot in the robot coordinate system and the desired heading angle is introduced as follows:

$${}^R\theta_{ir}^e = {}^R\theta_{ir} - {}^R\theta_{ir}^C, \tag{7}$$

where, ${}^{R}\theta_{ir}^{C}$ is the desired values of the heading angle of the ideal robot in the robot coordinate system.

Introducing Eq. 7 into Eq. 6 yields:

$$\begin{aligned}
{}^{R}\dot{x}_{ir} &= \frac{{}^{R}y_{ir}}{r_R}u_1 - u_2 + v_{ir}\cos{}^{R}\theta_{ir}, \\
{}^{R}\dot{y}_{ir} &= -\frac{{}^{R}x_{ir}}{r_R}u_1 - v_{ir}(\sin{}^{R}\theta_{ir} - \sin{}^{R}\theta_{ir}^{C}) - v_{ir}\sin(k_1{}^{R}\dot{y}_{ir}), \\
{}^{R}\dot{\theta}_{ir}^{e} &= \frac{u_1}{r_R} + \frac{k_1{}^{R}x_{ir}}{r_R}u_1 + k_1 v_{ir}\sin{}^{R}\theta_{ir}.
\end{aligned} \tag{8}$$

The Lyapunov function is constructed as follows:

$$V = ({}^{R}x_{ir})^2/2 + ({}^{R}y_{ir})^2/2 + ({}^{R}\theta_{ir}^{e})^2/2, \tag{9}$$

Differentiating the Lyapunov function, we obtain:

$$\begin{aligned}
\dot{V} &= {}^{R}\dot{x}_{ir}{}^{R}x_{ir} + {}^{R}\dot{y}_{ir}{}^{R}y_{ir} + {}^{R}\dot{\theta}_{ir}^{e}{}^{R}\theta_{ir}^{e} \\
&= -{}^{R}x_{ir}u_2 + {}^{R}x_{ir}v_{ir}\cos{}^{R}\theta_{ir} \\
&\quad -{}^{R}y_{ir}v_{ir}(\sin{}^{R}\theta_{ir} - \sin{}^{R}\theta_{ir}^{C}) \\
&\quad -{}^{R}y_{ir}v_{ir}\sin(k_1{}^{R}y_{ir}) + \frac{1 + k_1{}^{R}x_{ir}}{r_R}{}^{R}\theta_{ir}^{e}u_1 \\
&\quad +k_1{}^{R}\theta_{ir}^{e}v_{ir}\sin{}^{R}\theta_{ir}.
\end{aligned} \tag{10}$$

The η is introduced as follows:

$$\eta = (\sin{}^{R}\theta_{ir} - \sin{}^{R}\theta_{ir}^{C})/{}^{R}\theta_{ir}^{e}, \tag{11}$$

By substituting η into Eq. 10, we obtain:

$$\begin{aligned}
u_1 &= \frac{r_R}{1 + k_1{}^{R}x_{ir}}(-k_1 v_{ir}\sin{}^{R}\theta_{ir} - k_2{}^{R}\theta_{ir}^{e} + {}^{R}y_{ir}v_{ir}\eta), \\
u_2 &= v_{ir}\cos{}^{R}\theta + k_3{}^{R}x_{ir}.
\end{aligned} \tag{12}$$

Finally, we transform u_1 and u_2 into the direct control variables v_R and φ_R for the robot, yielding:

$$\begin{aligned}
v_R &= \sqrt{A + B}, \\
\varphi_R &= \arccos\frac{v_{ir}\cos{}^{R}\theta + k_3{}^{R}x_{ir}}{v_{ir}}.
\end{aligned} \tag{13}$$

where:

$A = r_R{}^2({}^{R}y_{ir}v_{ir}\eta - k_1 v_{ir}\sin{}^{R}\theta_{ir} - k_2{}^{R}\theta_{ir}^{e})^2/(1 + k_1{}^{R}x_{ir})^2$

$B = (v_{ir}\cos{}^{R}\theta + k_3{}^{R}x_{ir})^2$

At this point, the derivative of the Lyapunov function is:

$$\dot{V} = -{}^{R}y_{ir}v_{ir}\sin(k_1{}^{R}y_{ir}) - k_2({}^{R}\theta_{ir}^{e})^2 - k_3{}^{R}x_{ir}{}^2. \tag{14}$$

IV. EXPERIMENTAL RESULTS

This section introduces and discusses the experimental results of the proposed method through application.

A. Port terminal yard experiment

This section validates the proposed method through field experiments with a vehicle transport robot equipped with four multi-line LIDARs for real-time detection and a single-line LIDAR on the gripping mechanism for tire alignment. Point lasers ensure secure gripping. RTTMEC switches perception regions based on the robot's state, and TVPEA obtains the target pose. During docking, as the relative pose between the robot and the target vehicle changes, the contour of the target vehicle facing the robot varies. Accurate target pose estimation is crucial for docking control.

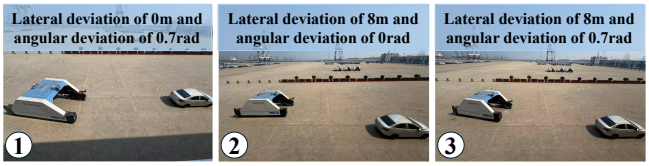

Fig. 4: Vehicle Transfer Robot Pickup Scene

TVPEA's effectiveness is first validated. To demonstrate RTTMEC's superiority, comparative experiments were conducted with three common methods: (1) SLTT, which plans a safe path using a pure trajectory tracking algorithm; (2) CCA, a correction docking algorithm based on angular and lateral deviations; and (3) BSTT, which plans a smooth docking curve using third-order B-spline interpolation and a pure trajectory tracking algorithm.

B. Performance analysis

The proposed method allowed the vehicle transport robot to complete tasks autonomously without human intervention. This section analyzes three experiments to assess the method's performance.

1) Experiment 1: Yard Vehicle Retrieval

In Fig. 4, three scenarios are examined for lateral and yaw angle deviations: 0 lateral and 0.7 rad yaw; 8 m lateral and 0 yaw; and 8 m lateral with 0.7 rad yaw. Fig. 5 shows TVPEA outcomes for 8 m lateral and 0.7 rad yaw deviations. Significant changes in x, y, and yaw angle of the target vehicle are detected by the robot at 40 s. The y change is most pronounced because the robot initially scans only the rear contour, with full contour scanning possible after 40 s. Maximum detection errors for x, y, and yaw angle are 0.32 m, 3.18 m, and -0.02 rad, respectively, with y deviation about half the vehicle length.

Fig. 6 shows the path and heading angle variation during docking in three scenarios. Fig. 7 presents the time taken to pick up and grasp the target car using different methods across ten scenarios. The robot remains in autonomous mode. In the first five scenarios, the initial angle deviation is 0, with lateral deviations of $4m$, $5m$, $6m$, $7m$, and $8m$. In the latter five, the initial angle deviation is 0.7 rad, with the same lateral deviations.

RTTMEC outperforms CCA and SLTT, generating docking paths with minimal deviations, approaching zero. BSTT takes the most time, significantly impacting efficiency due to the robot's large volume and complex kinematics, requiring extensive path planning. In contrast, RTTMEC, which avoids path planning, significantly reduces runtime, improving efficiency by 6.5%.

2) Experiment 2: Yard Vehicle Parking

In automobile terminal yards, densely packed vehicle storage areas are common. Robot parking relies on the arrangement of nearby parked vehicles to optimize space and conserve resources. Fig. 8 illustrates parking in a dense yard. The robot uses TVPEA to dynamically obtain positions

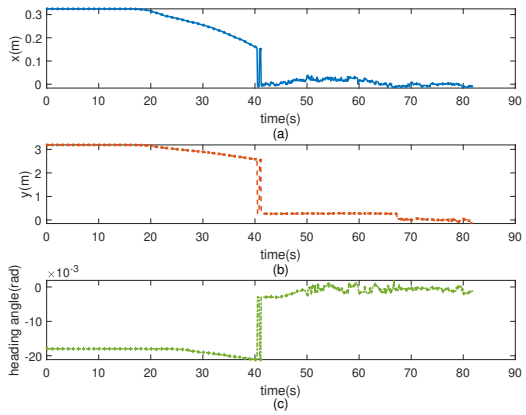

Fig. 5: Target Pose Detection under TVEPA. (a)The x of the target vehicle. (b)The x of the target vehicle. (c)The heading angle of the target vehicle.

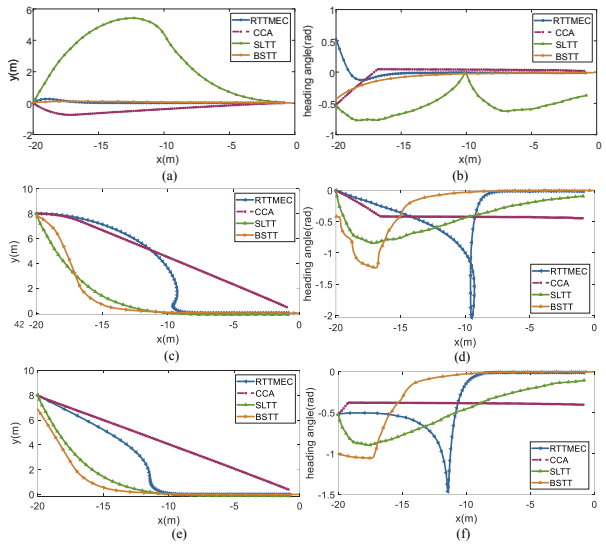

Fig. 6: Comparison of Driving Paths and Heading Angle Variations under Different Docking Algorithms. (a) Path with $0.7rad$ angular and $0m$ lateral deviation. (b) Heading angle with $0.7rad$ angular and $0m$ lateral deviation. (c) Path with $0rad$ angular and $8m$ lateral deviation. (d) Heading angle with $0rad$ angular and $8m$ lateral deviation. (e) Path with $0.7rad$ angular and $8m$ lateral deviation. (f) Heading angle with $0.7rad$ angular and $8m$ lateral deviation.

and orientations of vehicles on the left and right, estimates the parking area's pose, and utilizes RTTMEC to complete parking. As lateral and angular deviations approach zero, the robot scans vehicles ahead and around in real-time. When the distance between vehicles reaches 30, cm, the robot stops to complete parking.

Fig. 9 shows the point cloud and driving path of a robot placing vehicles in a dense yard, with the ideal path in red dots. Using laser radar, the robot acquires point cloud data, calculates the parking area's pose, and plans the ideal path. It then tracks this path, correcting deviations until docking is

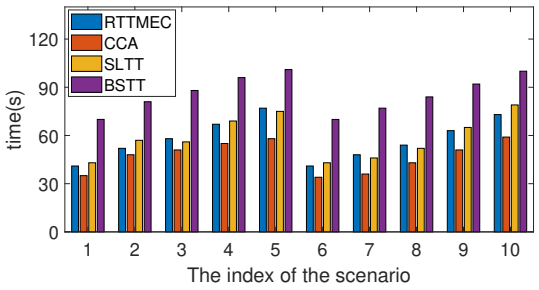

Fig. 7: Comparison of Docking Times under Different Docking Algorithms

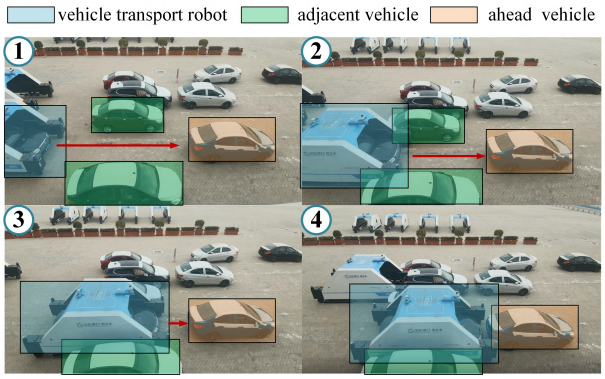

Fig. 8: Dense Area Vehicle Parking Experiment Scenario

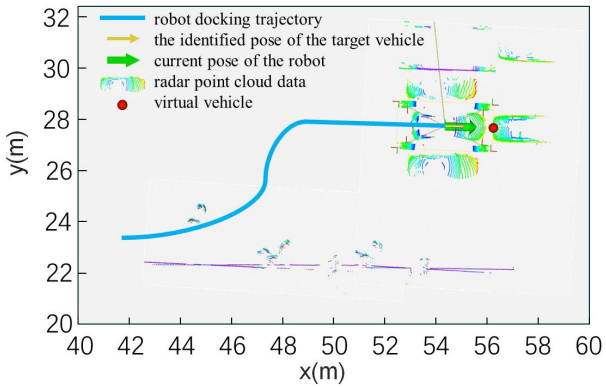

Fig. 9: Dense Area Vehicle Retrieval Path under RTTMEC

complete, resulting in precise and reliable vehicle placement.

3) Experiment 3: Compression Test

The vehicle transfer robot must execute back-and-forth operations for picking up and placing vehicles at the Ro/Ro terminal, requiring high stability in its control system. Fig. 10 show the lateral and longitudinal deviations between the target vehicle and the robot during 110 picking operations in a real outdoor scenario at the Ro/Ro terminal yard. These deviations, obtained from single-line LIDAR scans of vehicle tires on the robot's gripping mechanism, achieve millimeter-level accuracy.

As depicted in Fig. 10(a)(b), the lateral deviations between the robot and the target vehicle's front and rear wheels mostly range from -0.03 to 0.03, indicating high precision

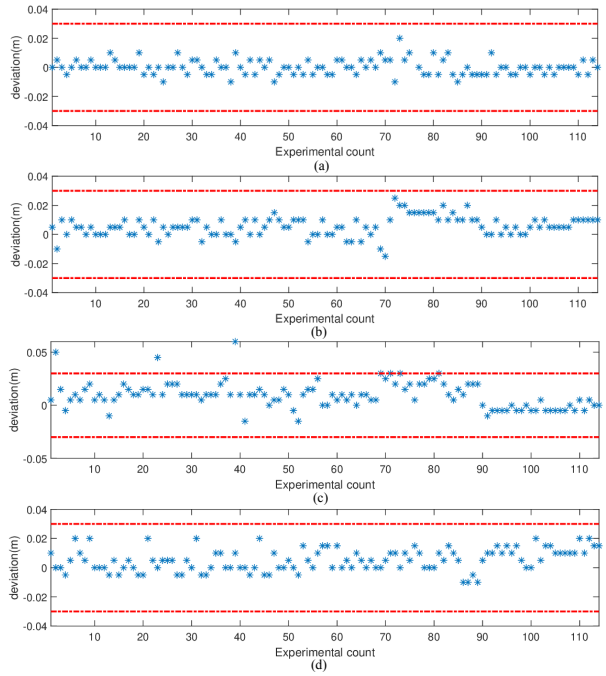

Fig. 10: Statistics of Final Deviation for 110 Vehicle Pickup Experiments. (a) Front Wheel Lateral Deviation. (b) Rear Wheel Lateral Deviation. (c) Front Wheel Longitudinal Deviation. (d) Rear Wheel Longitudinal Deviation

in the robot's picking and docking operations, meeting practical production requirements. Similarly, as shown in Fig. 10(c)(d), the longitudinal deviations, influenced by the robot's parking control and lateral movement control of the gripping mechanism, also predominantly range from -0.03 to 0.03.

V. CONCLUSION

This study proposes a novel control framework for a Straddle-Type Dual-Body vehicle transfer robot to meet the control requirements in roll-on/roll-off terminals. The framework includes perception area detection strategy switching, target pose estimation, and docking control. Tailored to the robot's structure, fine segmentation and processing of point clouds from different areas are performed, with perception strategies switched based on event triggers. A traversal-based point cloud matrix fitting algorithm is used for pose estimation. A docking controller, based on real-time target detection, minimizes lateral and angular errors during loading and unloading operations, ensuring precise and safe docking.

Experimental validation conducted in outdoor roll-on/roll-off terminal yards confirms the effectiveness of the proposed framework. Compared to traditional methods, there is a 6.5% improvement in operational efficiency, with docking deviations maintained within $3cm$ over 110 docking operations. The robot also performs effectively in dense unloading areas, highlighting the control framework's potential for addressing complex material handling tasks.

REFERENCES

[1] M. N. Abourraja, N. Rouky, M. Kornevs, S. Meijer, and N. Kringos, "A simulation-based decision support framework devoted to ro–ro terminals: Design, implementation and evaluation," vol. 180, 2023, p. 109248.

[2] J. Q. Dias, J. Calado, and M. Mendonça, "The role of european ro-ro port terminals in the automotive supply chain management," vol. 18, no. 1, 2010, pp. 116–124.

[3] A. Grau, M. Indri, L. Lo Bello, and T. Sauter, "Robots in industry: The past, present, and future of a growing collaboration with humans," vol. 15, no. 1, 2021, pp. 50–61.

[4] H. Martínez-Barberá and D. Herrero-Pérez, "Autonomous navigation of an automated guided vehicle in industrial environments," vol. 26, no. 4, August 2010, pp. 296–311.

[5] H. Martinez-Barbera and D. Herrero-Perez, "Development of a flexible agv for flexible manufacturing systems," vol. 37, no. 5, August 2010, pp. 459–468.

[6] M. De Ryck, M. Versteyhe, and F. Debrouwere, "Automated guided vehicle systems, state-of-the-art control algorithms and techniques," vol. 54, January 2020, pp. 152–173.

[7] Z. Slanina, I. Pergl, and P. Kedron, "Automated guided vehicle control system for automated parking purposes," vol. 55, no. 4, August 2022, pp. 362–367.

[8] P. Polack, L.-M. Dallen, and A. Cord, "Strategy for automated dense parking: how to navigate in narrow lanes," 2020, pp. 9196–9202.

[9] J. Zhang, Y. Chu, Z. Wang, T. Ye, L. Cai, and H. Yang, "Vehicle pose estimation system base on pressure sensor array for clamping parking robot," 2021, pp. 95–100.

[10] G. Serpen and C. Dou, "Automated robotic parking systems: real-time, concurrent and multi-robot path planning in dynamic environments," vol. 42, October 2015, pp. 231–251.

[11] G. Chen, J. Hou, J. Dong, Z. Li, S. Gu, B. Zhang, J. Yu, and A. Knoll, "Multiobjective scheduling strategy with genetic algorithm and time-enhanced a* planning for autonomous parking robotics in high-density unmanned parking lots," vol. 26, no. 3, September 2020, pp. 1547–1557.

[12] Y. Xu, Z. Chen, C. Deng, S. Wang, and J. Wang, "Lcdl: Towards dynamic localization for autonomous landing of unmanned aerial vehicle based on lidar-camera fusion," 2024, pp. 1–1.

[13] M. I. Pereira, R. M. Claro, P. N. Leite, and A. M. Pinto, "Advancing autonomous surface vehicles: A 3d perception system for the recognition and assessment of docking-based structures," vol. 9, 2021, pp. 53 030–53 045.

[14] W. Lin, A. Anwar, Z. Li, M. Tong, J. Qiu, and H. Gao, "Recognition and pose estimation of auto parts for an autonomous spray painting robot," vol. 15, no. 3, 2019, pp. 1709–1719.

[15] H.-Y. Lin, S.-C. Liang, and Y.-K. Chen, "Robotic grasping with multi-view image acquisition and model-based pose estimation," vol. 21, no. 10, 2021, pp. 11 870–11 878.

[16] W. Yin, H. Wen, Z. Ning, J. Ye, Z. Dong, and L. Luo, "Fruit detection and pose estimation for grape cluster–harvesting robot using binocular imagery based on deep neural networks," vol. 8, June 2021, p. 626989.

[17] M. B. Villalonga, A. Rodriguez, B. Lim, E. Valls, and T. Sechopoulos, "Tactile object pose estimation from the first touch with geometric contact rendering," in *Proceedings of the 2020 Conference on Robot Learning*, vol. 155, Nov 2021, pp. 1015–1029.

[18] Y. Wang, M. Shan, Y. Yue, and D. Wang, "Autonomous target docking of nonholonomic mobile robots using relative pose measurements," vol. 68, no. 8, June 2021, pp. 7233–7243.

[19] X. Zhang, X. Li, and X. Zhang, "Automatic docking and charging of mobile robot based on laser measurement," vol. 5, March 2021, pp. 2229–2234.

[20] E. Tsiogas, I. Kleitsiotis, I. Kostavelis, A. Kargakos, D. Giakoumis, M. Bosch-Jorge, R. J. Ros, R. L. Tarazón, S. Likothanassis, and D. Tzovaras, "Pallet detection and docking strategy for autonomous pallet truck agv operation," December 2021, pp. 3444–3451.

[21] J. Villagra and D. Herrero-Perez, "A comparison of control techniques for robust docking maneuvers of an agv," vol. 20, no. 4, July 2012, pp. 1116–1123.

[22] D. Herrero, J. Villagrá, and H. Martínez, "Self-configuration of waypoints for docking maneuvers of flexible automated guided vehicles," vol. 10, no. 2, Feb. 2013, pp. 470–475.

[23] M. Seelinger and J.-D. Yoder, "Automatic visual guidance of a forklift engaging a pallet," vol. 54, no. 12, Dec 2006, pp. 1026–1038.